Inorganic Chemistry

Article

pubs.acs.org/IC

Crystal Field Splitting of the Ground State of Terbium(III) and Dysprosium(III) Complexes with a Triimidazolyl Tripod Ligand and an Acetate Determined by Magnetic Analysis and Luminescence

Seira Shintoyo,[†] Keishiro Murakami,[†] Takeshi Fujinami,[†] Naohide Matsumoto,[†] Naotaka Mochida,[‡] Takayuki Ishida,[‡] Yukinari Sunatsuki,[§] Masayuki Watanabe,[∥] Masanobu Tsuchimoto,[⊥] Jerzy Mrozinski,[¶] Cecilia Coletti,[#] and Nazzareno Re*[,#]

[†]Department of Chemistry, Faculty of Science, Kumamoto University, Kumamoto 860-8555, Japan

[‡]Department of Engineering Science, The University of Electro-Communications, Chofu, Tokyo 182-8585, Japan

[§]Department of Chemistry, Faculty of Science, Okayama University, Tsushima-naka 3-1-1, Okayama 700-8530, Japan

[∥]Nuclear Science and Engineering Directorate, Japan Atomic Energy Agency, Tokai-mura 319-1195, Japan

[⊥]Department of Chemistry, Chiba Institute of Technology, Shibazono 2-1-1, Narashino, Chiba 275-0023, Japan

[¶]Faculty of Chemistry, University of Wroclaw, 14, F. Joliot-Curie, 50-383 Wroclaw, Poland

[#]Dipartimento di Farmacia, Università degli Studi "G.. D'Annunzio", I-66100 Chieti, Italy

Supporting Information

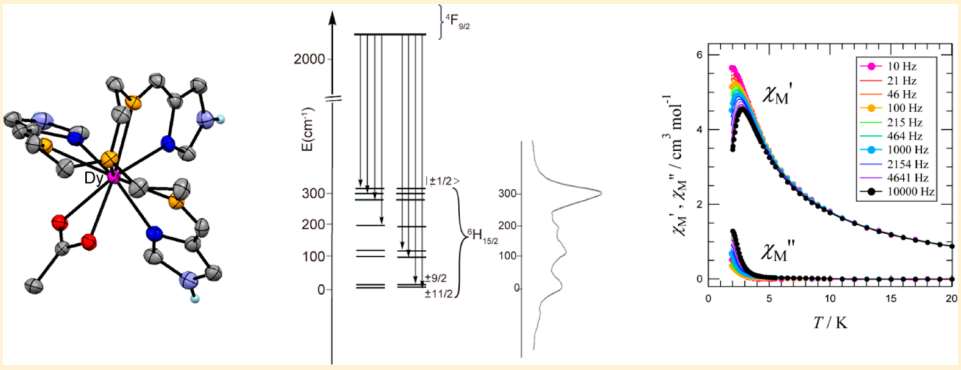

ABSTRACT: Terbium(III) and dysprosium(III) complexes with a tripodal N_7 ligand containing three imidazoles (H_3L) and a bidentate acetate ion (OAc^-), $[Ln^{III}(H_3L)(OAc)](ClO_4)_2{\cdot}MeOH{\cdot}H_2O$ (Ln = Tb, **1**; Ln = Dy, **2**), were synthesized and studied, where H_3L = tris[2-(((imidazol-4-yl)methylidene)amino)ethyl]amine. The Tb^{III} and Dy^{III} complexes have an isomorphous structure, and each Tb^{III} or Dy^{III} ion is coordinated by the tripodal N_7 and the bidentate acetate ligands, resulting in a nonacoordinated capped-square-antiprismatic geometry. The magnetic data, including temperature dependence of the magnetic susceptibilities and field dependence of the magnetization, were analyzed by a spin Hamiltonian, including the crystal field effect on the Tb^{III} ion ($4f^8$, $J = 6$, $S = 3$, $L = 3$, $g_J = 3/2$, $^7F_6$) and the Dy^{III} ion ($4f^9$, $J = 15/2$, $S = 5/2$, $L = 5$, $g_J = 4/3$, $^6H_{15/2}$). The Stark splittings of the ground states $^7F_6$ of the Tb^{III} ion and $^6H_{15/2}$ of the Dy^{III} ion were evaluated from the magnetic analyses, and the energy diagram patterns indicated an easy axis (Ising type) anisotropy for both complexes, which is more pronounced for **2**. The solid-state emission spectra of both complexes displayed sharp bands corresponding to the f−f transitions, and the fine structures assignable to the $^5D_4 \rightarrow {}^7F_6$ transition for **1** and the $^6F_{9/2} \rightarrow {}^6H_{15/2}$ transition for **2** were related to the energy diagram patterns from the magnetic analyses. **1** and **2** showed an out-of-phase signal with frequency dependence in alternating current (ac) susceptibility under a dc bias field of 1000 Oe, indicative of a field-induced SIM.

INTRODUCTION

Since the discovery of single-molecule magnets (SMMs) from a Mn_{12} cluster,[1] SMMs consisting of transition-metal clusters,[2] lanthanide complexes,[3] and lanthanide−transition-metal complexes[4] have been extensively studied during the last two decades. Since the easy-axis magnetic anisotropy required for SMM behavior can be easily generated for some lanthanide ions by the crystal field (CF) effect, lanthanide complexes are good candidates for SMMs. In fact, it has been reported that a number of lanthanide complexes, including mononuclear[5] and polynuclear[6] complexes, showed SMM properties, and some of them exhibited high blocking temperatures and large relaxation barriers. SMM behavior is determined by an energy diagram of

Received: June 18, 2014
Published: September 9, 2014

Scheme 1. Structures of (a) $[Ln^{III}(H_3L)(OAc)]^{2+}$ with a Tripodal N_7 Ligand and an Acetate Ion and (b) Capped Square Antiprism of $[Ln^{III}(H_3L)(OAc)]^{2+}$ Viewed along the Direction from a Central Amine Nitrogen to the Ln^{III} Ion[a]

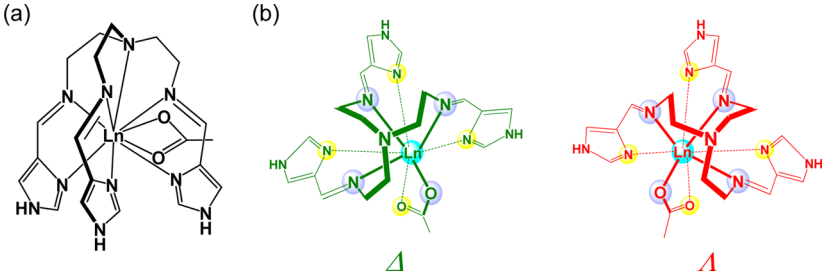

[a]Chiral Δ and Λ enantiomorphs are due to the clockwise and anticlockwise arrangements of the tripodal ligand around the Ln^{III} ion, respectively.

the ground state in which the splitting of the ground multiplet stabilizes the sublevels with the largest $|J_z|$ value and assumes a significant energy gap from the first excited sublevel. The f−f transition of the emission spectrum gives a direct picture of the ground-state splitting, and if the f−f transition is observed and the fine structure is well-resolved, the splitting of the ground J multiplet can be determined by spectral analysis. However, the emission spectrum of the f−f transition associated with well-resolved fine structure has been rarely observed, especially for the magnetically relevant Dy^{III} complex.[7,8]

From the viewpoint of determining the energy diagram by the analysis of the magnetic behavior and of the emission spectrum, we have synthesized a series of lanthanide complexes which exhibit strong and well-resolved f−f transitions.[9] For polynuclear lanthanide complexes,[6] such an analysis is prevented by the entangling of the CF effect of the single lanthanide ions and of the interion f−f exchange coupling. For mononuclear lanthanide complexes,[5] single ion magnet (SIM) behavior is due only to the CF splitting of the lowest J multiplet, and therefore a study of mononuclear lanthanide complexes with varying coordination geometries allows the establishment of a correlation among the CF effect, the ground-state splitting, and their SIM behavior.

In previous studies, mononuclear Tb^{III} complexes with different coordination geometries of similar ligands and the resolved f−f emission spectra were synthesized.[9] The study of the Tb^{III} complexes "*fac*"-$[Tb^{III}(HL^{DL\text{-}ala})_3]\cdot 7H_2O$ and "*mer*"-$[Tb^{III}(HL^{DL\text{-}phe})_3]\cdot 7H_2O$, where $HL^{DL\text{-}ala}$ = *N*-[(imidazol-4-yl)methylidene]-DL-alanine and $HL^{DL\text{-}phe}$ = *N*-[(imidazol-4-yl)methylidene]-DL-phenylalanine, showed a good correlation between the energy diagram pattern obtained from the analysis of the magnetic and luminescence properties and the observed SIM behavior.

In this study, Tb^{III} and Dy^{III} complexes with a tripodal N_7 ligand containing three imidazoles (H_3L = tris[2-(((imidazol-4-yl)methylidene)amino)ethyl]amine) and a bidentate acetate ion (OAc^-), $[Tb^{III}(H_3L)(OAc)](ClO_4)_2\cdot MeOH\cdot H_2O$ (**1**) and $[Dy^{III}(H_3L)(OAc)](ClO_4)_2\cdot MeOH\cdot H_2O$ (**2**), have been synthesized and their structures and magnetic and luminescent properties have been investigated with the support of DFT calculations (Scheme 1). The use of this tripodal ligand by our group has led to many advantages in the design of functional inorganic complexes and materials exhibiting novel architectures and electronic, optical, and magnetic phenomena. We have reported a series of transition-metal Cu^{II}, Ni^{II}, Fe^{II}, Fe^{III}, and Co^{III} complexes, which showed spin crossover, pH-dependent chromism, various assembly structures made by imidazole−imidazolate and imidazole−chloride hydrogen bonds, and chiral discrimination leading to spontaneous resolution.[10,11] Lanthanide complexes with the same ligand also showed interesting properties such as high stability in dilute acetonitrile, methanol, and aqueous solutions due to the encapsulation of the lanthanide ion which also leads to strong luminescence in solution, spontaneous resolution in the solid state, and the synthesis of simple model compounds whose ground-state splitting can be studied by the magnetic susceptibility and luminescence spectra.[9,12] Previously, we reported the syntheses, crystal structures, and luminescence spectra of several Eu^{III}, Sm^{III}, and Tb^{III} complexes of the same and analogous tripodal N_7 ligands and one of them, $[Eu^{III}(H_3L)(OAc)](ClO_4)_2\cdot H_2O$, is isostructural with **1** and **2**.[13a]

The magnetic data, including temperature dependence of the magnetic susceptibilities and field dependence of the magnetization, were analyzed by a spin Hamiltonian including the crystal field effect on the Tb^{III} ion for **1** and the Dy^{III} ion for **2**. The ground state of the Tb^{III} ion ($4f^8$, $J = 6$, $S = 3$, $L = 3$, $g_J = 3/2$) is $^7F_6$, and the crystal field effect on the Tb^{III} ion removes the degeneracy of the 13 components of $|J, J_z\rangle = |6, J_z\rangle$ ($J_z = \pm 6, \pm 5, \pm 4, \pm 3, \pm 2, \pm 1, 0$) (known as the Stark splitting). The ground state of the Dy^{III} ion ($4f^9$, $J = 15/2$, $S = 5/2$, $L = 5$, $g_J = 4/3$, $^6H_{15/2}$) is $^6H_{15/2}$, and analogously, the CF effect removes the degeneracy of the 16 components of $|J_z\rangle = |15/2, J_z\rangle$ ($J_z = \pm 15/2, \pm 13/2, \pm 11/2, \pm 9/2, \pm 7/2, \pm 5/2, \pm 3/2, \pm 1/2$). The Stark splittings of the ground states $^7F_6$ of the Tb^{III} ion and $^6H_{15/2}$ of the Dy^{III} ion were evaluated from the magnetic analyses, and the energy diagram patterns indicate an easy-axis (Ising type) anisotropy. The solid-state emission spectra of both complexes display sharp bands corresponding to the f−f transitions, and the fine structures assigned to the $^5D_4 \rightarrow {}^7F_6$ transition for **1** and the $^6F_{9/2} \rightarrow {}^6H_{15/2}$ transition for **2** were related to the energy diagram patterns from the magnetic analyses of crystal field calculations. Complexes **1** and **2** showed an out-of-phase signal with frequency dependence in alternating current (ac) susceptibility under a dc bias field of 1000 Oe, indicative of a field-induced SIM. We report here the synthesis, structures, luminescent and magnetic properties, and DFT calculations of **1** and **2**.

EXPERIMENTAL SECTION

Caution! The perchlorate salts of metal complexes with organic ligands are potentially explosive. Only small quantities of the compound should be prepared, and they should be handled with much care.

Materials. All reagents and solvents in the syntheses were of reagent grade, available from Tokyo Kasei Co., Ltd. and Wako Pure Chemical Industries, Ltd. These were used without further

dx.doi.org/10.1021/ic501453h | *Inorg. Chem.* 2014, 53, 10359−10369

purification. All reactions were carried out under an ambient atmosphere.

$[Tb^{III}(H_3L)(OAc)](ClO_4)_2\cdot MeOH\cdot H_2O$ (1). Complex **1** was prepared by a method adopted for the corresponding Eu^{III} complex.[13] A solution of tris(2-aminoethyl)amine (0.073 g, 0.5 mmol) in 10 mL of methanol and a solution of 4-formylimidazole (0.144 g, 1.5 mmol) in 10 mL of methanol were mixed, and the mixture was stirred at 50 °C for 1 h and then cooled to room temperature. To the resultant ligand solution (H_3L) was added a solution of $Tb^{III}(OAc)_3\cdot 4H_2O$ (0.204 g, 0.5 mmol) in 10 mL of water, and the mixture was stirred for 30 min at room temperature. A solution of $NaClO_4$ (0.122 g, 1 mmol) in 10 mL of water was added, and the resultant mixture was stirred for 30 min and then filtered. The filtrate was left to stand for a few days to form colorless crystals. The crystals exhibit efflorescence, and the elemental analysis agreed with the chemical formula with $[Tb^{III}(H_3L)(OAc)](ClO_4)_2\cdot MeOH\cdot H_2O$. Yield: 0.222 g (53%). Anal. Calcd for $[Tb^{III}(H_3L)(OAc)](ClO_4)_2\cdot MeOH\cdot H_2O$, $C_{20}H_{27}N_{10}O_{10}Cl_2Tb\cdot MeOH\cdot H_2O$: C, 29.77; H, 3.93; N, 16.53. Found: C, 29.63; H, 3.91; N, 16.64. IR (KBr, cm^{-1}): ν(C=N) 1645, $\nu_a(COO^-)$ 1540, $\nu_s(COO^-)$ 1459, ν (ClO_4^-) 1087. Single-crystal X-ray analysis revealed that the crystal contains one methanol and one water molecule per complex. TGA was carried out between room temperature and 115 °C by the use of a small amount of a freshly prepared crystalline sample: two-step weight loss (1.5% and 3.5%) was observed in the heating mode. In the cooling mode, the sample absorbs the vapor to increase the weight from −3.5% to −1.2%.

$[Dy^{III}(H_3L)(OAc)](ClO_4)_2\cdot MeOH\cdot H_2O$ (2). Complex **2** was prepared in a way similar to that for **1**, using $Dy^{III}(OAc)_3\cdot 4H_2O$, instead of $Tb^{III}(OAc)_3\cdot 4H_2O$. Yield: 0.153 g (36%) as colorless crystals. Anal. Calcd for $[Dy^{III}(H_3L)(OAc)](ClO_4)_2\cdot MeOH\cdot H_2O$, $C_{20}H_{27}N_{10}O_{10}Cl_2Dy\cdot MeOH\cdot H_2O$: C, 29.64; H, 3.91; N, 16.46. Found: C, 29.43; H, 4.04; N, 16.36. IR (KBr, cm^1): ν(C=N) 1645, $\nu_a(COO^-)$ 1542, $\nu_s(COO^-)$ 1461, ν (ClO_4^-) 1089. TGA of freshly prepared sample: 4.5% two-step weight loss was observed in the heating mode from room temperature to 115 °C. In the cooling mode, the sample absorbs the vapor to increase the weight from −4.5% to −2.5%.

Physical Measurements. Elemental C, H, and N analyses were carried out at the Center for Instrumental Analysis of Kumamoto University. Infrared spectra recorded at room temperature were obtained using a JEOL JIR-6500W spectrometer with samples in KBr disks. Thermogravimetric analyses (TGA) were performed on a TG/DTA6200 (Seiko Instrument Inc.). Due to the potential explosion of the perchlorate salt, a small amount of the sample (ca. 3 mg) was used. The samples were heated from room temperature to 115 °C in the heating mode at a heating rate of 5 °C min^{-1}, kept at that temperature for 30 min, and then cooled to room temperature. High-resolution luminescence spectra were measured with a Horiba Fluoromax-4P spectrometer at 77 K. A quartz tube (o.d. 8 mm) was used as a powder cell fixed in a quartz Dewar sample holder filled with liquid nitrogen. Excitation slits of 1 and 2 nm and emission slits of 1 and 0.5 nm were used for **1** and **2**, respectively. Temperature-dependent magnetic susceptibilities in the temperature range 1.9−300 K at an external magnetic field of 0.1 T and field-dependent magnetization measurements in an applied magnetic field from 0 to 5 T at 1.9 K were measured with an MPMS XL5 SQUID susceptometer (Quantum Design, Inc.). All samples were fixed with a small amount of liquid paraffin to avoid orientation in the field. The calibrations were performed with palladium. Corrections for diamagnetism were applied using Pascal's constants.[14] ac magnetic susceptibility was measured on a PPMS ac/dc magnetometer (Quantum Design, Inc.) in a temperature range down to 1.9 K at 0 and 1000 Oe dc fields.

X-ray Crystal Structure Analysis. The single-crystal X-ray diffraction data of **1** and **2** were collected by a Rigaku RAXIS RAPID imaging plate diffractometer using graphite-monochromated Mo Kα radiation (λ = 0.71073 Å) at 150 K. The temperature of the crystal was maintained within an accuracy of ±2 K by a Rigaku N_2 cryostat. The structures were solved by direct methods and expanded using the Fourier technique.[15] Hydrogen atoms were located at calculated positions and refined using a riding model. All calculations were performed using the CrystalStructure crystallographic software package.[16] The crystallographic data and the relevant coordination bond distances with the hydrogen bond distances are given in Tables 1 and 2, respectively.

Table 1. X-ray Crystallographic Data for 1 and 2 at 150 K

	1	2
formula	$C_{21}H_{33}O_{12}N_{10}Cl_2Tb$	$C_{21}H_{33}O_{12}N_{10}Cl_2Dy$
formula wt	847.38	850.95
cryst syst	monoclinic	monoclinic
space group	$P2_1/c$ (No. 14)	$P2_1/c$ (No. 14)
a, Å	17.1674(5)	17.1562(4)
b, Å	10.5558(4)	10.5875(2)
c, Å	17.4175(6)	17.3802(4)
β, deg	92.9486(8)	93.2036(7)
V, Å^3	3152.16(17)	3152.01(11)
Z	4	4
D_{calcd}, g cm^{-3}	1.785	1.793
μ, cm^{-1}	24.83	26.18
R,[a] R_w[b]	0.0526, 0.1618	0.0352, 0.1197

[a] $R = \sum||F_o| - |F_c||/\sum|F_o|$. [b] $R_w = [\sum(w(F_o^2 - F_c^2)^2)/\sum w(F_o^2)^2]^{1/2}$.

Table 2. Coordination Bond Distances (Å) and Bond Angles (deg) for 1 and 2 at 150 K

	1	2
	Bond Lengths	
Ln−N(1)	2.671(5)	2.649(4)
Ln−N(2)	2.493(5)	2.475(4)
Ln−N(3)	2.520(5)	2.515(4)
Ln−N(5)	2.500(5)	2.492(3)
Ln−N(6)	2.542(5)	2.524(3)
Ln−N(8)	2.507(5)	2.503(3)
Ln−N(9)	2.494(5)	2.483(4)
Ln−O(9)	2.447(4)	2.430(3)
Ln−O(10)	2.441(4)	2.426(3)
	Bond Angles	
N(2)−Ln−N(5)	89.1(1)	88.7(1)
N(2)−Ln−N(8)	130.7(1)	131.5(1)
N(3)−Ln−N(6)	70.5(1)	70.4(1)
N(3)−Ln−N(9)	106.3(1)	105.2(1)
N(5)−Ln−N(8)	77.0(1)	77.0(1)
N(6)−Ln−N(9)	73.0(1)	72.4(1)

DFT Calculations. DFT (density functional theory) unrestricted calculations were performed with the Jaguar 7.9 quantum chemistry package[17] using B3LYP-D3: i.e., the B3LYP functional with Grimme's ab initio long-range dispersion corrections.[18] This functional is known to give a good performance at a reasonable computational cost for the description of large systems, where noncovalent interactions may play an important role, generally dealt with heavy highly correlated techniques. The Cundari−Stevens ECP basis set,[19] also called csdz, was employed for the terbium(III) and dysprosium(III) ions. This set provides a good description for lanthanides, using an effective core potential for the inner core electrons and treating outer core and valence electrons with a 4s/4p/2d/2f basis set. Main-group atoms were described by a 6-31G(p) basis set.

RESULTS AND DISCUSSION

Synthesis and Characterization of $[Tb^{III}(H_3L)(OAc)](ClO_4)_2\cdot MeOH\cdot H_2O$ (1) and $[Dy^{III}(H_3L)(OAc)](ClO_4)_2\cdot MeOH\cdot H_2O$ (2). Previously, we reported the syntheses, crystal structures, and luminescence spectra of a Eu^{III} complex of the same tripodal N_7 ligand possessing three imidazole groups (see

dx.doi.org/10.1021/ic501453h | Inorg. Chem. 2014, 53, 10359−10369

Scheme 1a) and demonstrated that the Eu^{III} complex encapsulated by the tripodal ligand is actively luminescent even in a dilute acetonitrile solution (1.0×10^{-5} M).[13a] Complexes **1** and **2** were prepared by a method reported for the Eu^{III} and Sm^{III} complexes with the same or analogous tripodal ligands.[13] The tripodal Schiff-base ligands H_3L were prepared by the 1:3 condensation reaction of tris(2-aminoethyl)amine and 4-formylimidazole. A solution of $Ln^{III}(OAc)_3{\cdot}4H_2O$ (Ln^{III} = Tb^{III}, Dy^{III}) was added to the ligand solution, followed by the addition of a solution of $NaClO_4$ in a mixed solution of methanol and water. Colorless crystals precipitated from the reaction mixture. The elemental analyses agreed with the formula of $[Ln^{III}(H_3L)(OAc)](ClO_4)_2{\cdot}MeOH{\cdot}H_2O$ (Ln = Tb, Dy). Single-crystal X-ray analyses revealed that the Tb^{III} and Dy^{III} complexes have structures isomorphous with that of the corresponding Eu^{III} complex.[13a] TGA of a freshly prepared crystalline sample shows weight loss corresponding to the crystal solvent. For **1**, a total 3.5% weight loss was observed in the heating mode from room temperature to 115 °C. In the cooling mode, the sample absorbs the vapor to increase the weight from −3.5% to −1.2%. The 3.5% weight loss is due to the methanol (calculated value 3.7%) and the 2.3% weight increase in the cooling mode is due to the vapor absorption of one water molecule per complex (calculated value 2.1%). For **2**, 4.6% weight loss was observed in the heating mode from room temperature to 115 °C. In the cooling mode, the sample absorbs the vapor to increase the weight from −4.6% to −2.4%. The 4.6% weight loss is due to the elimination of one methanol and a half-molecule of water (calculated value 4.8%) and the 2.2% weight increase in the cooling mode is due to the vapor absorption of one water molecule per complex (calculated value 2.1%). The IR spectra showed a sharp band at ca. 1645 cm^{-1} assignable to the C═N stretching vibration of a Schiff base ligand. The strong absorptions at ca. 1540 and 1459 cm^{-1} are assigned to $\nu_a(COO^-)$ and $\nu_s(COO^-)$ of the bidentate acetate moiety, respectively. The broad and strong absorptions around 1100 cm^{-1} are characteristic of perchlorate ion.

Crystal Structures of 1 and 2. Compounds **1** and **2** crystallized in the centrosymmetric monoclinic space group $P2_1/c$ (No. 14), and has a structure isomorphous to that of the corresponding Eu^{III} complex of formula $[Eu^{III}(H_3L)(OAc)](ClO_4)_2{\cdot}H_2O$, differing only for a crystallization solvent molecule.[13a] Crystallographic data are given in Table 1. The relevant coordination bond distances and angles are given in Table 2. As the two compounds are isomorphous with each other and have the same structural features, the crystal structure of **2** is exemplified and described in detail. The structure consists of the complex cation $[Dy^{III}(H_3L)(OAc)]^{2+}$, two ClO_4^- counteranions, and one methanol and one water molecule as the crystallization solvents. The molecular structure of $[Dy^{III}(H_3L)(OAc)]^{2+}$ with the selected atom-numbering scheme is shown in Figure 1. The Dy^{III} ion is coordinated by nine donor atoms consisting of seven nitrogen atoms of the tripodal heptadentate ligand (H_3L; three imidazole, three imine, and one central amine nitrogen) and two oxygen atoms of an acetate ion. The Dy−N(1) distance of 2.649(4) Å (where N(1) is the central amine nitrogen) is longer than the other six Dy−N distances, which are in the ranges 2.475(4)−2.503(3) Å for Dy−N(imine) and 2.483(4)−2.524(3) Å for the Dy−N(imidazole) bonds. An acetate ion coordinates to the Dy^{III} ion in a bidentate mode (with Dy−O distances of 2.430(3) and 2.426(3) Å). The tripodal ligand encapsulates one Dy^{III} ion by

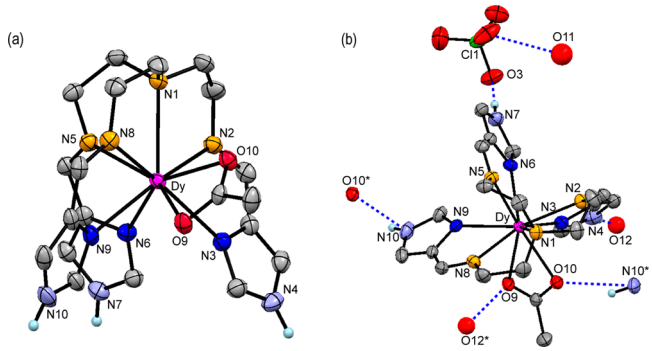

Figure 1. (a) Molecular structure of $[Dy^{III}(H_3L)(OAc)]^{2+}$ of **2** with the selected atom-numbering scheme. Hydrogen atoms, except for the imidazole hydrogen atoms, are omitted for clarity. (b) Molecular structure of $[Dy^{III}(H_3L)(OAc)]^{2+}$ projected along the direction from the central amine nitrogen N(1) to the Dy^{III} ion, showing a capped square antiprism and the hydrogen bonds between the cation $[Dy^{III}(H_3L)(OAc)]^{2+}$ and ClO_4^-, H_2O, and MeOH.

the seven nitrogen atoms, but the geometry is significantly distorted from C_3 symmetry due to the insertion of a bidentate OAc^- ligand between N(3) and N(9) of imidazole nitrogen atoms and between N(2) and N(8) of imine nitrogen atoms, as shown in Figure 1b. As evidenced by the three N(imidazole)−Dy−N(imidazole) angles N(3)−Dy−N(6) = 70.4(1)°, N(3)−Dy−N(9) = 105.2(1)°, and N(6)−Dy−N(9) = 72.4(1)°, the N(3)−Dy−N(9) angle is much larger than the other two angles, because of the inserted coordination of an acetate ion between N(3)−Dy−N(9). The d-transition-metal complexes such as those of Fe^{II}, Fe^{III}, and Co^{III} with the same tripodal ligand have a six-coordinated octahedral coordination geometry by N_6 donor atoms with nearly C_3 symmetry, where the central amine N is not bound, and the N(imidazole)−M−N(imidazole) angles are nearly equivalent.[10]

The coordination polyhedra of the $Ln^{III}N_7O_2$ were approximately assigned by using the continuous shape-measure theory and SHAPE software[20] for Ln = Tb^{III}, Dy^{III}, together with the previously reported analogue, Ln^{III} = Eu^{III}.[13a] The calculation indicated that the $Ln^{III}N_7O_2$ coordination polyhedra were intermediate between a spherical capped square antiprism (CSA) and a spherical tricapped trigonal prism (TCTP) (shape measures were 1.759 and 1.728, respectively, for Ln^{III} = Tb^{III}, 1.678 and 1.621, respectively, for Ln^{III} = Dy^{III}, and 1.818 and 1.924 for Ln = Eu^{III}) (see Scheme 2).

In the CSA structure, the central amine nitrogen N(1) occupies the capped position, the upper square consists of one

Scheme 2. Sketches of (a) Capped-Square-Antiprismatic (CSA) and (b) Tricapped-Trigonal-Prismatic (TCTP) Coordination Geometries

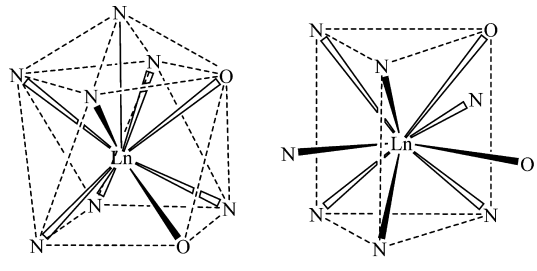

dx.doi.org/10.1021/ic501453h | Inorg. Chem. 2014, 53, 10359−10369

acetate oxygen O(10) and the three imine nitrogen atoms N(2), N(5), and N(8), and the bottom square consists of one acetate oxygen O(9) and the three imidazole nitrogen atoms N(3), N(6), and N(9). In the spherical tricapped trigonal prism, the top and bottom trigonal faces consist of the three atoms N(1), N(8), and O(10) and the three atoms N(6), N(9), and N(3), respectively. The three tricapped positions are occupied by N(2), N(5), and O(9). The differences between the two polyhedra seem to be slight.[21]

As shown in Figure 1b, the three imidazole groups (N(4), N(7), N(10)) of the $[Dy^{III}(H_3L)(OAc)]^{2+}$ cation are hydrogen bonded to a water molecule O(12) with N(4)···O(12) = 2.676(5) Å, to an oxygen atom of a perchlorate anion with N(7)···O(3) = 2.984(5) Å, and to one of the acetate oxygen atoms of the adjacent cation with N(10)···O(10)* = 2.841(5) Å, respectively. The intermolecular imidazole···acetate hydrogen bond N(10)···O(10)* is repeated to produce a one-dimensional chain structure running along the *c* axis. Owing to the screw coordination arrangement of the tripodal ligand with respect to the Dy^{III} ion, there are two possible optical isomers, i.e., Δ and Λ enantiomorphs. Two adjacent molecules in a chain are related by a symmetry operation of the *c* glide plane, and the Δ and Λ isomers are alternately arrayed in the chain to form a heterochiral chain. These adjacent chains thus generated are running along opposite directions and are linked by a water molecule O(12) through two hydrogen bonds of O(9) ··· O(12) = 2.735(5) Å and N(4)···O(12) = 2.676(5) Å to form a ladder structure (see Figure 2).

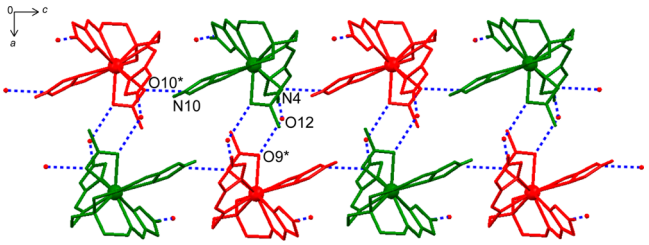

Figure 2. Ladder structure of **2** along the *c* axis, where ClO_4^- and MeOH are omitted for clarity and these species are not involved in the formation of the dimensional structure. Adjacent chains are linked by a water molecule O(12) through two hydrogen bonds of O(9)···O(12) and N(4)···O(12) to form a ladder-type structure with the heterochiral dimer structure unit $\{[Dy^{III}(H_3L)(OAc)]^{2+}\cdots O(12)\}$.

Magnetic Properties of 1 and 2. The temperature dependences of dc magnetic susceptibilities in the temperature range of 1.9−300 K and the field dependences of the magnetization at 1.9 K in the range 0−5 T were measured for **1** and **2**, and the results are shown in Figure 3 as $\chi_M T$ vs T and M vs H plots.

The $\chi_M T$ values of 12.25 and 14.48 cm^3 K mol^{-1} at room temperature for Tb^{III} and Dy^{III} complexes are close to the values of 11.82 and 14.17 cm^3 K mol^{-1} in the free ion approximation, expected for a Tb^{III} ion ($4f^8$, $J = 6$, $S = 3$, $L = 3$, $g_J = 3/2$, $^7F_6$) and Dy^{III} ion ($4f^9$, $J = 15/2$, $S = 5/2$, $L = 5$, $g_J = 4/3$, $^6H_{15/2}$), respectively, according to the formula[14]

$$\chi_M T = \frac{N g_J{}^2 \beta^2}{3k} J(J+1)$$

The decrease in the low-temperature region is due to the crystal field effect on the Ln^{III} ion that removes the degeneracy of the $2J + 1$ components of the $^{2S+1}L_J$ ground state, $|J,J_z\rangle = |6,J_z\rangle$ (J_z = ±6, ±5, ±4, ±3, ±2, ±1, 0) for the $^7F_6$ ground state of Tb^{III} for **1** and $|J,J_z\rangle = |15/2,J_z\rangle$ (J_z = ±15/2, ±13/2, ±11/2, ±9/2, ±7/2, ±5/2, ±3/2, ±1/2) for the $^6H_{15/2}$ ground state of Dy^{III} for **2**, into a series of sublevels (known as Stark splitting) whose width is of the order of 100 cm^{-1}. Therefore, while at room temperature most sublevels are populated and the free ion value is approached, when the temperature is lowered the highest levels are depopulated and $\chi_M T$ decreases.[14]

In order to quantify the magnetic anisotropy of these complexes, the temperature dependence of $\chi_M T$ and the field dependence of M were analyzed using a spin Hamiltonian approach and taking into account the crystal field. A detailed analysis of the crystal field effect on the Ln^{III} would require the diagonalization of the spin Hamiltonian

$$\mathbf{H} = \beta(\mathbf{L}_{Ln} + 2\mathbf{S}_{Ln})H + \mathbf{H}_{cf}(Ln) \quad (1)$$

in which the crystal field interaction contribution is represented by the equation using the Stevens operators $\mathbf{H}_{cf} = \sum_{k=2,4,6}\sum_{q=0}^{k} B_k{}^q \mathbf{O}_k{}^q$.[22,23] Although several excited states should in principle be included in magnetic analysis of lanthanide compounds, the magnetic behavior in the temperature range where only the Stark sublevels of the ground state are populated could be well reproduced considering solely the ground-state components and employing the spin equivalent operator approach. Moreover, to avoid overparameterization,

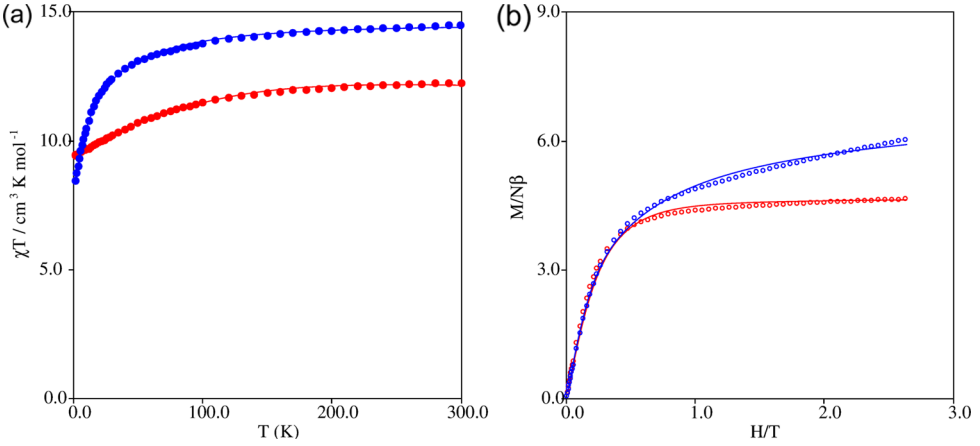

Figure 3. Plots of (a) the temperature dependence of $\chi_M T$ and (b) the field dependence of $M/N\beta$ at 1.9 K for complexes **1** (red) and **2** (blue). The solid lines represent the theoretical curves with the best-fit parameters given in the text.

dx.doi.org/10.1021/ic501453h | Inorg. Chem. 2014, 53, 10359−10369

we considered only the axial anisotropy terms, corresponding to the Stevens operators $\mathbf{O}_2^0$, $\mathbf{O}_4^0$, and $\mathbf{O}_6^0$, which can be expressed as polynomials of the total angular momentum operators $\mathbf{J}^2$ and $\mathbf{J}_z$. This choice reduces the anisotropy parameters from 15 to 3 and is justified by the distorted C_4 crystal field symmetry around the lanthanide ion (approximately D_{4d}, taking into account the much longer Ln−N(1) bond). Moreover, such a choice has often been employed to reproduce the magnetic behavior of Tb^{III} and Dy^{III} complexes.[3a,b,5a,24] The magnetic behavior of **1** and **2** was therefore analyzed with the Hamiltonian

$$\mathbf{H} = \beta H g_J \mathbf{J}_{Ln} + B_2^0\mathbf{O}_2^0 + B_4^0\mathbf{O}_4^0 + B_6^0\mathbf{O}_6^0 \quad (2)$$

where H denotes the applied magnetic field, β is the Bohr magneton, and B_2^0, B_4^0, and B_6^0 are the axial anisotropy parameters of the Ln^{III} ion. According to the Abragam and Bleaney notation, the anisotropy parameters B_k^q are related to the LF parameters, also employed in the molecular magnetism literature, by the equation $B_k^q = A_k^q\langle r^k\rangle\theta_k$, where θ_k values are the Stevens coefficients.[23]

The temperature dependence of $\chi_M T$ for **1** in the whole temperature range was analyzed with the Hamiltonian (2); although several fits corresponding to a minimum of the agreement factor $R = \sum(\chi_M T_{obsd} - \chi_M T_{calcd})^2/\sum(\chi_M T_{calcd})^2$ were actually found, all with almost the same values of g_J and B_2^0 and differing mainly in the B_4^0 and B_6^0 values, the best fit compatible with the M vs H behavior and the luminescence spectra (see below) was obtained with the fitting parameters g_J = 1.52, B_2^0/k_B = −1.24 K, B_4^0/k_B = 0.032 K, and B_6^0/k_B = +5.8 × 10^{-5} K, shown as solid line in Figure 3a.

The field dependence of the magnetization at 1.9 K from 0 to 5 T for **1** (see Figure 3b) shows that, upon an increase in the applied external magnetic field, the magnetization increases to 4.66$N\beta$ at 5 T without reaching the expected saturation value of 9$N\beta$. This is again due to the crystal field effect on the Tb^{III} ion that removes the 13-fold degeneracy of the $^7F_6$ ground state. A reasonable agreement is observed between the curves obtained with the Hamiltonian of eq 2 and the same parameters obtained from fit of magnetic susceptibilities (see solid lines in Figure 3b), although an accurate fit requires an adjustment of the B_2^0, B_4^0, and B_6^0 parameters leading to B_2^0/k_B = −1.19 K, B_4^0/k_B = 0.041 K, and B_6^0/k_B = +4.6 × 10^{-5} K.

The temperature dependence of $\chi_M T$ for **2** in the whole temperature range was analyzed with Hamiltonian (2); although several fits corresponding to a minimum of the agreement factor $R = \sum(\chi_M T_{obsd} - \chi_M T_{calcd})^2/\sum(\chi_M T_{calcd})^2$ were actually found, all with almost the same values of g_J and B_2^0 and differing mainly in the B_4^0 and B_6^0 values, the best fit compatible with the M vs H behavior and the luminescence spectra (see below) was obtained with the fitting parameters g_J = 1.35, B_2^0/k_B = −0.63 K, B_4^0/k_B = 0.017 K, and B_6^0/k_B = −1.6 × 10^{-5} K, and the theoretical curve is shown as a solid line in Figure 3 (a).

The field dependence of the magnetization from 0 to 5 T for **2** was measured at 1.9 K; the $M/N\beta$ vs H plot is reported in Figure 3b and shows that, upon an increase in the applied external magnetic field, the magnetization increases to 6.04$N\beta$ at 5 T without reaching the expected saturation value of 10$N\beta$. This is again due to the crystal field effect on the Dy^{III} ion that removes the 16-fold degeneracy of the $^6H_{15/2}$ ground state. A reasonable agreement is observed between the curves obtained with the Hamiltonian of eq 2 and the same parameters obtained from fit of magnetic susceptibilities (see solid lines in Figure 3b), although an accurate fit requires an adjustment of the B_2^0, B_4^0, and B_6^0 parameters leading to B_2^0/k_B = −0.81 K, B_4^0/k_B = 0.012 K, and B_6^0/k_B = −2.1 × 10^{-5} K.

The calculated B_k^q parameters are resumed in Table 3 together with the corresponding CF parameters $A_k^q\langle r^k\rangle\theta_k$, and their values are of the same orders of magnitude as those reported for other Tb^{III} and Dy^{III} complexes with N and O donor atoms,[3a,b,5a,24] including a few complexes with similar square-antiprismatic coordination.[3a,b,24]

Table 3. Magnetic Anisotropy Parameters Obtained for Complexes 1 and 2[a]

anisotropy param	1	2
g_J	1.52	1.35
B_2^0/k_B	−1.24	−0.63
$A_2^0\langle r^2\rangle/k_B$	+120	+100
B_4^0/k_B	+0.032	−0.017
$A_4^0\langle r^2\rangle/k_B$	+260	−290
B_6^0/k_B	+5.8 × 10^{-5}	−1.5 × 10^{-5}
$A_6^0\langle r^2\rangle/k_B$	−50	−10

[a]All values are in K except for g_J.

The diagram of the multiplet energy levels of the ground state $^7F_6$ of Tb^{III} ion for **1** and that of the ground state $^6H_{15/2}$ of Dy^{III} ion for **2** are represented in parts a and b of Figure 4, respectively. First of all we notice that, owing to the use of a simplified spin Hamiltonian containing only axial terms, all components with the same $|M_J|$ values are degenerate so that the sublevels originating from the splitting of both ground states under the CF effect are made up of $|\pm M_J\rangle$ pseudodoublets, except the $|0\rangle$ sublevel for Tb^{III}.

The diagram of **1** shows the $|\pm5\rangle$ doublet as the ground state, with the first excited state, $|\pm4\rangle$, almost degenerate, at only 2 cm^{-1}, while the remaining sublevels are well above, from $|\pm3\rangle$ at 90 cm^{-1} to the highest level, $|0\rangle$, at 268 cm^{-1}, which defines the total Stark splitting. Such an energy level pattern indicates an easy axis anisotropy of the Tb^{III} ion and is compatible with a SIM behavior, although the splitting of the first excited state is very low. For **2**, the ground state corresponds to the $|\pm11/2\rangle$ doublet with the first excited state, $|\pm9/2\rangle$, at only 8 cm^{-1}, while the remaining components are above 100 cm^{-1} with the highest multiplet level, $|\pm1/2\rangle$, significantly mixed with $|\pm3/2\rangle$ at 338 cm^{-1}, which therefore defines the total Stark splitting. Such an energy level pattern indicates an essentially easy axis anisotropy of the Dy^{III} ion and is compatible with a SIM behavior, although the splitting of the first excited state is quite low.

Luminescent Properties of 1 and 2. The photographs of the solid samples of **1** and **2** at room temperature under the irradiation of UV light (365 nm) are shown in parts a and b of Figure 5, respectively. Efficient f−f emissions were observed even for the Dy^{III} complex **2**, while generally the emission of the Dy^{III} complex is not observed or is very weak.[7,8] Parts a and b of Figure 5 show the f−f emission spectra of **1** and **2** recorded in the solid state at 77 K upon irradiation of UV light at 312 and 308 nm, respectively.

For the Tb^{III} complex **1**, the emission bands were found at ca. 490 (20.4 × 10^3), 545 (18.3 × 10^3), 590 (16.9 × 10^3), 630 (15.9 × 10^3), 650 (15.3 × 10^3), 670 (14.9 × 10^3), and 680 (14.7 × 10^3) nm (cm^{-1}), which were attributed to the f−f transitions $^5D_4 \rightarrow {}^7F_J$, with J = 6−0, respectively. Each band

dx.doi.org/10.1021/ic501453h | Inorg. Chem. 2014, 53, 10359−10369

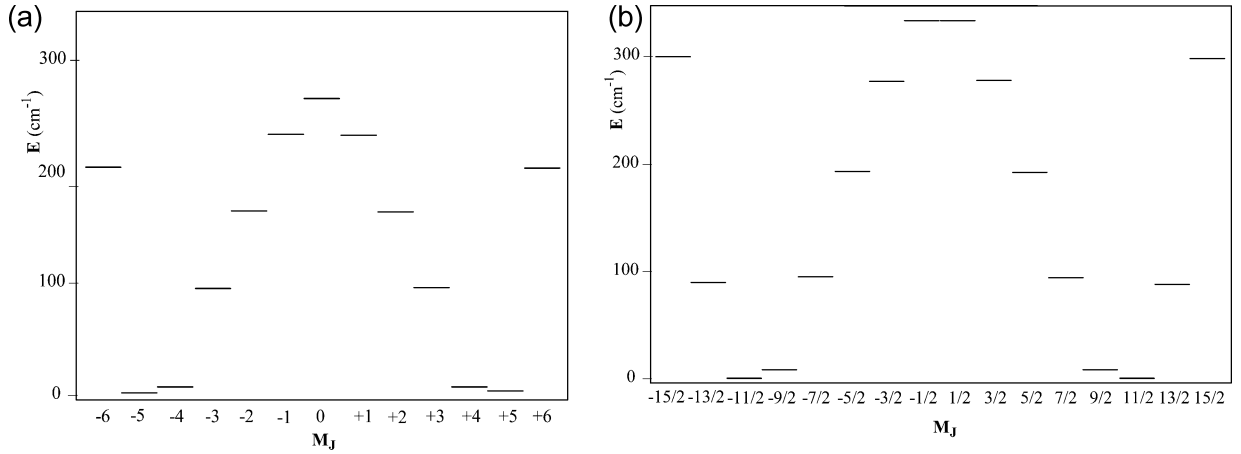

Figure 4. (a) Energy levels obtained from the magnetic analysis derived from the splitting of (a) the ground state $^7F_6$ of the Tb^{III} ion in **1** and (b) the ground state $^6H_{15/2}$ of the Dy^{III} ion in **2**.

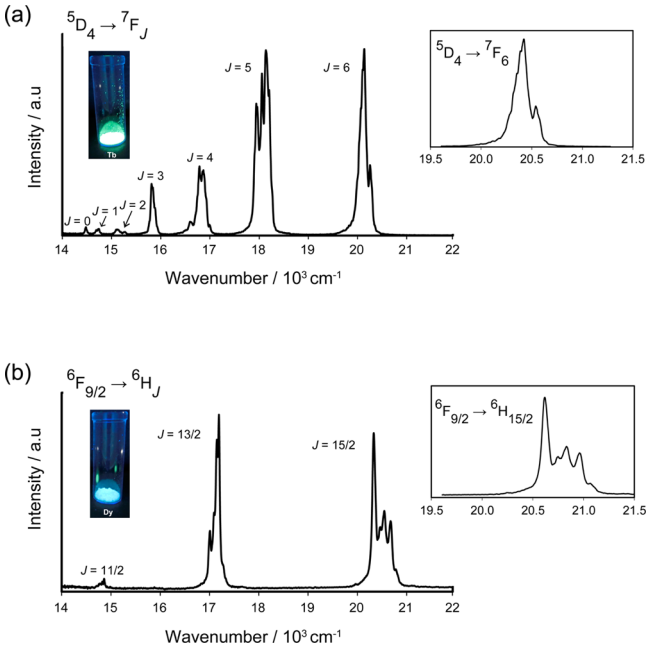

Figure 5. (a) Photograph of the solid sample of **1** at room temperature under the irradiation of 365 nm UV light and the emission spectrum of **1** by irradiation at 312 nm recorded at 77 K, with transition assignments. The fine structure of the $^5D_4 \rightarrow {}^7F_6$ band is shown in the inset. (b) Photograph of the solid sample of **2** at room temperature under the irradiation of 365 nm UV light and the emission spectrum of **2** by irradiation at 308 nm recorded at 77 K, with transition assignments. The fine structure of the $^6F_{9/2} \rightarrow {}^6H_{15/2}$ band is shown in the inset.

exhibited a fine structure with several peaks. The emission band at 490 nm is assigned to the $^5D_4 \rightarrow {}^7F_6$ transition, and its fine structure is due to the Stark splitting of the ground state $^7F_6$. Indeed, the emission spectrum is a direct picture of the ground-state Stark multiplet originating from the $^7F_6$ state: the highest energy peak of the band corresponds to the transition to the lowest sublevel, while the lowest energy peak corresponds to the transition to the highest sublevel. For the $^5D_4 \rightarrow {}^7F_6$ transition, two wide peaks were observed at ca. 487 (20.5×10^3) and 490 (20.4×10^3) nm (cm^{-1}), with several weak shoulders on the low energy side, and the deconvolution of the spectrum indicates six components at 20.540×10^3, 20.422×10^3, 20.388×10^3, 20.356×10^3, 20.316×10^3, and 20.261×10^3 cm^{-1}, which should be correlated with the splitting of the ground $^7F_6$ multiplet.

For the Dy^{III} complex **2**, the emission bands were found at ca. 480 (20.8×10^3), 575 (17.4×10^3), and 670 (14.9×10^3) nm (cm^{-1}), which were attributed to the f–f transitions $^6F_{9/2} \rightarrow {}^6H_J$, with J = 15/2, 13/2, 11/2, respectively. Each band exhibited a fine structure with several peaks. The emission band at 480 nm is assigned to the $^6F_{9/2} \rightarrow {}^6H_{15/2}$ transition, and its fine structure is due to the Stark splitting of the ground state $^6H_{15/2}$. Again, the emission spectrum is a direct picture of the ground-state Stark multiplet originating from the $^6H_{15/2}$ state. For the $^6F_{9/2} \rightarrow {}^6H_{15/2}$ transition, five peaks were observed at 475.0 (sh), 477.0, 479.8, 481.7, and 485.0 nm, and the deconvolution of the spectrum indicates five components at 21.066×10^3, 20.960×10^3, 20.833×10^3, 20.751×10^3, and 20.619×10^3 cm^{-1}, which should be correlated with the splitting of the ground $^6H_{15/2}$ multiplet.

A consistent assignment of the components observed in the highest energy band of the emission spectra can be carried out from the comparison with the energy diagram obtained from the fitting of the magnetic susceptibility measurements. The comparison for **1** is illustrated in Figure 6a and allows us to assign the two wide emission peaks of the $^5D_4 \rightarrow {}^7F_6$ band to two groups of sublevels close in energy, namely $|\pm5\rangle$ and $|\pm4\rangle$ for the peak at 487 nm, and $|\pm6\rangle$, $|\pm3\rangle$, $|\pm2\rangle$, $|\pm1\rangle$, and $|0\rangle$ for the peak at 490 nm. In particular, the six components obtained from the deconvolution (vide supra) can be assigned, in order of decreasing energy, to transitions from the excited $^5D_4$ state to a superposition of $|\pm5\rangle$ and $|\pm4\rangle$ and to the isolated $|\pm3\rangle$, $|\pm2\rangle$, $|\pm6\rangle$, $|\pm1\rangle$ and $|0\rangle$ components. This assignment is supported by a fairly good agreement of the energy differences between proposed transitions and observed peaks (with deviation below 40 cm^{-1}), in particular for the total splitting: 268 cm^{-1} vs 279 cm^{-1}.

The comparison for **2** requires, first of all, to take into account the presence of "hot" bands, involving excited components of the $^4F_{9/2}$ manifold as the starting level, which are quite common for Dy^{III} complexes.[8] Although the observed components of the $^4F_{9/2} \rightarrow {}^6H_{15/2}$ transition are less than the maximum expected number of eight peaks, the shape of the emission and the analogy with previous assignments of the emission spectra of other Dy^{III} mononuclear complexes[8] suggest assignment of the weak peak at the highest energy of

dx.doi.org/10.1021/ic501453h | Inorg. Chem. 2014, 53, 10359–10369

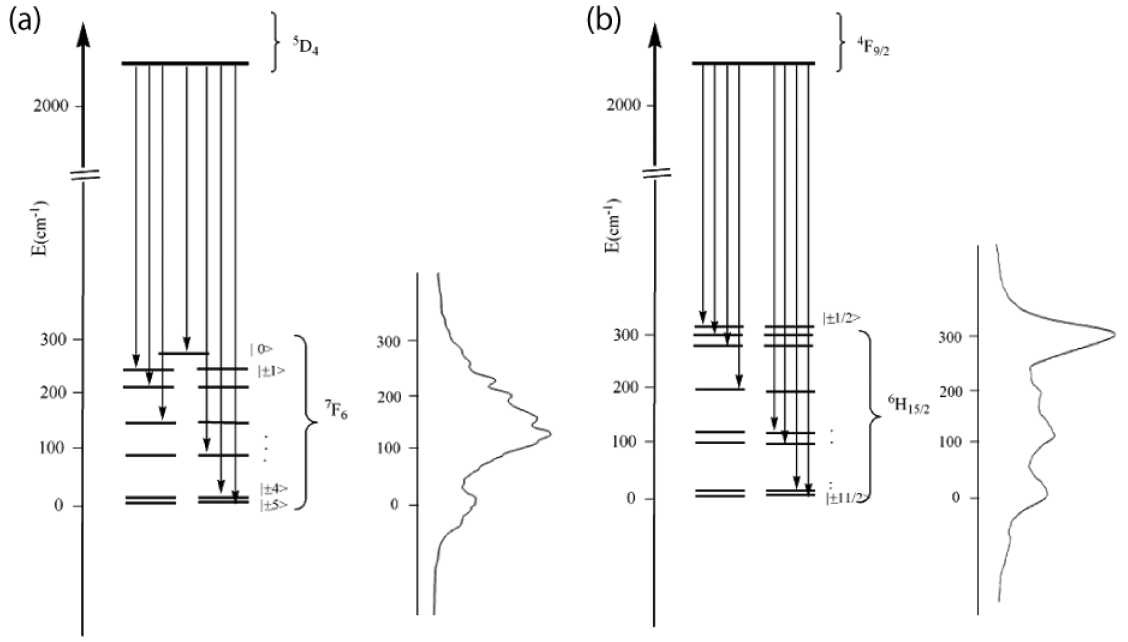

Figure 6. (a) Comparison of the Stark splitting of the $^7F_6$ ground state of the Tb^{III} ion from the magnetic analysis for **1** and the splitting observed from the emission f–f spectrum. (b) Comparison of the Stark splitting of the $^6H_{15/2}$ ground state of the Dy^{III} ion from the magnetic analysis for **2** and the splitting observed from the emission f–f spectrum.

2, at 21.066×10^3 cm^{-1}, to a hot band. The final comparison is illustrated in Figure 6b and allows us to assign the remaining four emission lines of the $^4F_{9/2} \rightarrow {}^6H_{15/2}$ band for **2** to transitions from the excited $^4F_{9/2}$ state to (i) a superposition of $|\pm 11/2\rangle$ and $|\pm 9/2\rangle$, (ii) a superposition of $|\pm 13/2\rangle$ and $|\pm 7/2\rangle$, (iii) the isolated $|\pm 5/2\rangle$, and (iv) a superposition of $|\pm 3/2\rangle$, $|\pm 15/2\rangle$, and $|\pm 1/2\rangle$ components. Beyond a good agreement of the energy differences between proposed transitions and observed peaks (with deviations below 30 cm^{-1}), we also notice a good agreement between the number of components involved in the proposed transitions and the intensity of the corresponding peaks.

The agreement between magnetic and fluorescence properties is reasonably good for both **1** and **2** and supports the Stark splitting of the J_z sublevels of the Tb^{III} and Dy^{III} ions and the nature of their magnetic anisotropy.

ac Magnetic Properties of 1 and 2. The dynamic magnetic properties of **1** and **2** were investigated by using ac magnetic susceptibility measurements. The in-phase (χ_M') and out-of-phase (χ_M'') components exhibit no frequency dependence in a zero bias field (Figure S3, Supporting Information) but become significantly more intense with the application of an external bias field of 1000 Oe, indicative of field-induced SIM. The temperature dependences of the ac magnetic susceptibilities under 1000 Oe dc field for **1** and **2** are shown in parts a and b of Figure 7, respectively.

No peak was found in χ_M'' down to 2 K for **1** or **2**, and accordingly the conventional Arrhenius plot could not be applied here. A modified Arrhenius analysis is available to estimate the activation energy (Δ) for the magnetization reorientation, by using the $\ln(\chi_M''/\chi_M')$ vs T^{-1} plots (Figure 8a,b). The Δ value and pre-exponential factor τ_0 are defined as $\ln(\chi_M''/\chi_M') = \ln(\omega\tau_0) + \Delta/k_BT$.[25] The optimized parameters are $\Delta/k_B = 3.2(8)$ K and $\tau_0 = [1.0(6)] \times 10^{-6}$ s for **1** and $\Delta/k_B = 8.5(2)$ K and $\tau_0 = [1.6(11)] \times 10^{-7}$ s for **2**. The energy barrier Δ is significantly larger for the Dy^{III} complex **2** than for the Tb^{III} complex **1** (8.5(2) vs 3.2(8) K). The magnitude of τ_0 is reasonable for SMM for each complex, and the τ_0 value of **2** is smaller than that of **1** by 1 order of magnitude.

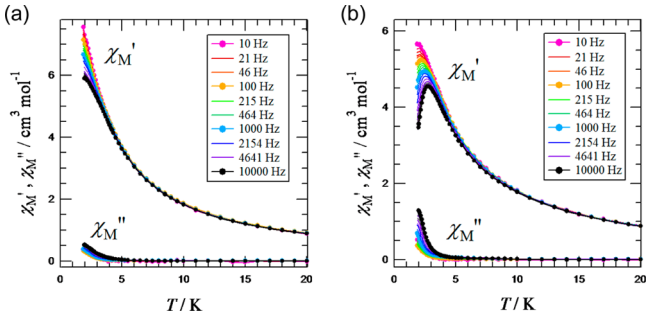

Figure 7. Temperature dependence of the in-phase (χ_M') and out-of-phase (χ_M'') ac susceptibility signals of **1** (a) and **2** (b) measured under various frequencies and under a 1000 Oe external dc field.

Figure 8c,d shows the Cole–Cole plots under 1000 Oe for **1** and **2**, respectively. There seem to be two independent relaxation processes in the magnetization relaxation in **1**. The origin of this anomaly can hardly be explained in terms of a typical SIM behavior with a simple double-well potential pattern (Figure 4a). One possible explanation is as follows. It may be related to the coexistence of pseudopolymorphs on the basis of the degree of solvation after storage, giving a superposition of two semicircle contributions. The coexistence of pseudopolymorphs also accounts for too many resolved lines in the emission spectra of **1** (Figure 6a). The Arrhenius parameters derived from Figure 8a can be regarded approximately as an average from two unresolved values. On the other hand, the plot for **2** shows a monotonous curve at any temperature, suggesting the presence of a unique relaxation process. The α parameter in the Debye model[2] could not be given because of the only partial semicircles obtained for **2**.

From the discussion above, we see that the prediction from the energy diagrams based on the CF calculation (Figure 4) is realized in the ac magnetic susceptibility measurements. Indeed,

dx.doi.org/10.1021/ic501453h | Inorg. Chem. 2014, 53, 10359–10369

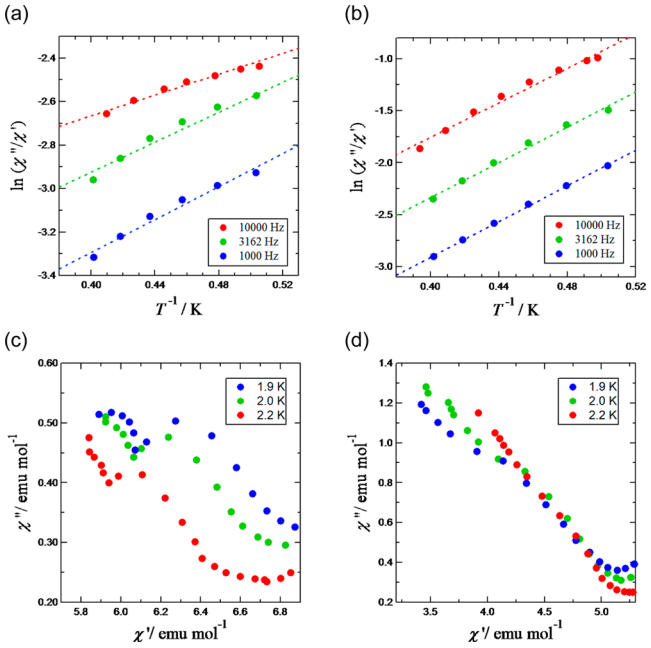

Figure 8. Modified Arrhenius plots for (a) **1** and (b) **2**. Dotted lines give linear fits. For the equation and optimized parameters, see the text. Cole−Cole plots for (c) **1** and (d) **2**.

a magnetic easy-axis anisotropy is suggested by approximate double-well potential curves for both **1** and **2** and both compounds actually exhibit an indication of SIM behavior around 2 K. Moreover, the small activation energies observed from the relaxation dynamics (8.5(2) vs 3.2(8) K), significantly higher for **2**, would be consistent with the estimated energy level patterns, provided the relaxation mechanism consists of a phonon-assisted tunneling process with a dominant contribution from the first excited doublet, at 2 cm^{-1} for **1** and 8 cm^{-1} for **2**.

DFT Calculations on 1 and 2. In order to point out the reasons behind the magnetic behavior and Stark splitting pattern of **1** and **2**, showing an easy-axis character for both compounds, we performed DFT calculations on the ligand environment aiming to estimate the electrostatic potential acting on the Tb^{III} and Dy^{III} ions, which is responsible for the CF acting on them. Indeed, the CF acting on a lanthanide ion determines the kind and the strength of its magnetic anisotropy; in particular, a strong easy-axis anisotropy is achieved when the CF stabilizes the ground sublevels with the highest $\pm M_J$ value. For both the $^7F_6$ ground state of Tb^{III} and the $^6H_{15/2}$ ground state of Dy^{III}, the components with the highest M_J values are known to have oblate spheroidal electronic distribution (that is, they have a larger electron distribution on the equatorial plane than on the principal axis) and are therefore expected to be stabilized by CFs originating from a ligand negative charge distribution with a dipolar character, i.e. with large negative charges from donor atoms located around the principal axis, leading to an easy-axis anisotropy.[26]

DFT calculations with the B3LYP-D3 functional were carried out on the ligand's environment, excluding the Tb^{III} or Dy^{III} ion, using the geometry from the X-ray analysis, and the resulting Mulliken analysis clearly shows that the negative charges on the acetate oxygen (−0.58/−0.59 e) are significantly larger than those on the amine (−0.53 e), imine (−0.51/−0.50 e), and imidazole (−0.47/−0.48 e) nitrogen atoms. Their position determines the anisotropy of the negative charge distribution and therefore of the electrostatic potential acting on the lanthanide ion. As shown in Figure 9 (geometries are

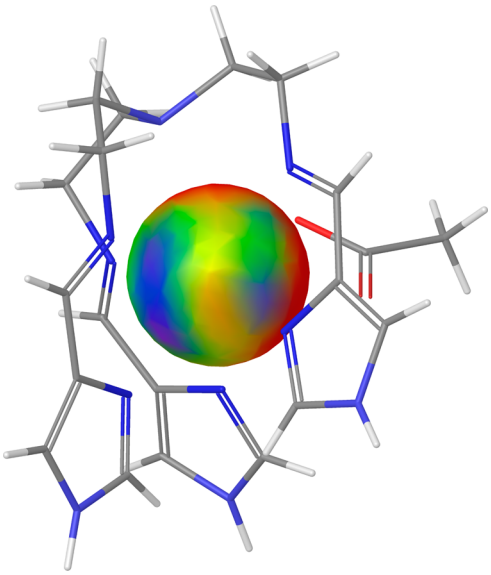

Figure 9. Ligand electrostatic potential projected on a sphere of radius 2 Å centered at the lanthanide ion position. Red and blue correspond to a more negative and a less negative electrostatic potential, respectively.

almost indistinguishable for the two complexes), the corresponding molecular electrostatic potential acting on the lanthanide ions has a feeble uniaxial distribution, indicating a weak stabilization of the components with the highest $\pm M_J$ values and therefore a magnetic easy-axis character.

Figure 9 shows the consequence of this charge arrangement on the electrostatic potential on a sphere centered in the lanthanide position. Indeed, there is a less negative electrostatic region originating from the imidazole nitrogen atoms, a slightly more negative region corresponding to the amine nitrogen, and a significantly more negative region originating from the negative carboxylate oxygen atoms. The region of high (red) electrostatic potential is therefore partially located on two almost separate sides. Thus, the electrostatic potential has a significant dipolar character, indicating a stabilization of the sublevels with the highest $\pm M_J$ value and therefore a magnetic easy-axis character. The high electrostatic potential regions are, however, quite spread on the sphere and are not well separated on opposite sides, so that the stabilization of the highest $\pm M_J$ sublevel is expected to be small and the anisotropy is weak, consistent with the low activation barriers observed for the magnetization reorientation. These results indicate that a careful analysis of the negative charge distribution around the lanthanide ion from DFT calculations allows us to give a rationale for the behavior of mononuclear complexes, opening the way to a rational design of anisotropic properties of lanthanide complexes and ultimately of their SIM behavior.

CONCLUSION

In this study, the Tb^{III} and Dy^{III} complexes with a tripodal N_7 ligand containing three imidazoles (H_3L = tris[2-(((imidazol-4-yl)methylidene)amino)ethyl]amine) and a bidentate acetate ion (OAc^-), have been synthesized and their structures and

dx.doi.org/10.1021/ic501453h | Inorg. Chem. 2014, 53, 10359−10369

magnetic and luminescent properties have been investigated. The analysis of magnetic data with a spin Hamiltonian including the crystal field effect on the Tb^{III} and Dy^{III} ions allowed us to evaluate the Stark splitting of their ground states, $^7F_6$ and $^6H_{15/2}$, and the resulting energy diagram patterns indicate a significant stabilization of the sublevels with large $|J_z|$ values and therefore an easy-axis (Ising type) anisotropy. The double-well potential pattern of the energy levels was supported by DFT calculations. The energy diagrams from the magnetic analysis were compared with the low-temperature emission spectra of the f−f transition of **1** and **2**, which showed the fine structures of the highest energy $^5D_4 \rightarrow {}^7F_6$ and $^6F_{9/2} \rightarrow {}^6H_{15/2}$ transitions, giving a direct picture of the ground-state splitting, and a good accord was observed. Both complexes showed a frequency-dependent out-of-phase signal in alternating current (ac) susceptibility under a dc bias field of 1000 Oe, indicative of field-induced SIM with small activation barriers. The combined analysis of the fast relaxation dynamics of the ac behavior and the detailed pattern of the energy diagrams evaluated from magnetic and luminescent properties suggests that the relaxation mechanism consists of a phonon-assisted tunneling process with a dominant contribution from the first excited doublet. This report shows that mononuclear lanthanide complexes exhibiting well-resolved fine structure in the f−f transition provide a suitable compound to establish a correlation between the CF splitting of the ground state and its magnetic properties.

■ ASSOCIATED CONTENT

Ⓢ Supporting Information

Figures giving TGA results and temperature and frequency dependences of the ac magnetic susceptibilities at 0 dc bias field and CIF files giving and X-ray crystallographic data (CIF) for **1** and **2**. This material is available free of charge via the Internet at http://pubs.acs.org. The X-ray crystallographic data in CIF format have also been deposited with the CCDC (reference numbers CCDC 985147 and 985148). They can be obtained free of charge via http://www.ccdc.cam.ac.uk/conts/retrieving.html or from the Cambridge Crystallographic Data Centre, 12 Union Road, Cambridge CB2 1EZ, U.K.: fax, (+44) 1223-336-033; e-mail, deposit@ccdc.cam.ac.uk.

■ AUTHOR INFORMATION

Corresponding Author

*E-mail for N.R.: nre@unich.it.

Notes

The authors declare no competing financial interest.

■ ACKNOWLEDGMENTS

T.F. was supported by the Research Fellowship of the Japan Society for the Promotion of Science, KAKENHI 00248556.

■ REFERENCES

(1) (a) Sessoli, R.; Gatteschi, D.; Caneschi, A.; Novak, M. A. *Nature* **1993**, *365*, 141−143. (b) Gatteschi, D.; Caneschi, A.; Pardi, L.; Sessoli, R. *Science* **1994**, *265*, 1054−1058. (c) Sessoli, R.; Tsai, H. L.; Schake, A. R.; Wang, S.; Vincent, J. B.; Folting, K.; Gatteschi, D.; Christou, G.; Hendrickson, D. N. *J. Am. Chem. Soc.* **1993**, *115*, 1804−1816. (d) Thomas, L.; Lionti, F.; Ballou, R.; Gatteschi, D.; Sessoli, R.; Barbara, B. *Nature* **1996**, *383*, 145−147. (e) Boskovic, C.; Brechin, E. K.; Streib, W. E.; Folting, K.; Bollinger, J. C.; Hendrickson, D. N.; Christou, G. *J. Am. Chem. Soc.* **2002**, *124*, 3725−3736.

(2) (a) Gatteschi, D.; Sessoli, R. *Angew. Chem., Int. Ed.* **2003**, *42*, 268−297. (b) Christou, G. *Polyhedron* **2005**, *24*, 2065−2075. (c) Gatteschi, D.; Sessoli, R.; Villain, J. *Molecular Nanomagnets*; Oxford University Press: Oxford, U.K., 2006. (d) Bagai, R.; Christou, G. *Chem. Soc. Rev.* **2009**, *38*, 1011−1026.

(3) (a) Ishikawa, N.; Sugita, M.; Ishikawa, T.; Koshihara, S.; Kaizu, Y. *J. Am. Chem. Soc.* **2003**, *125*, 8694−8695. (b) Ishikawa, N.; Sugita, M.; Okubo, T.; Tanaka, N.; Iino, T.; Kaizu, Y. *Inorg. Chem.* **2003**, *42*, 2440−2446. (c) Ishikawa, N.; Mizuno, Y.; Takamatsu, S.; Ishikawa, T.; Koshihara, S. Y. *Inorg. Chem.* **2008**, *47*, 10217−10219. (d) Woodruff, D. N.; Winpenny, R. E. P.; Layfield, R. A. *Chem. Rev.* **2013**, *113*, 5110−5148. (e) Habib, F.; Murugesu, M. *Chem. Soc. Rev.* **2013**, *42*, 3278−3288. (f) Zhang, P.; Guo, Y.-N.; Tang, J. *Coord. Chem. Rev.* **2013**, *257*, 1728−1763.

(4) (a) Osa, S.; Kido, T.; Matsumoto, N.; Re, N.; Pochaba, A.; Mrozinski, J. *J. Am. Chem. Soc.* **2004**, *126*, 420−421. (b) Hamamatsu, T.; Yabe, K.; Towatari, M.; Matsumoto, N.; Re, N.; Pochaba, A.; Mrozinski, J. *Bull. Chem. Soc. Jpn.* **2007**, *80*, 523−529. (c) Costes, J.-P.; Dahan, F.; Wernsdorfer, W. *Inorg. Chem.* **2006**, *45*, 5−7. (d) Ferbinteanu, M.; Kajiwara, T.; Choi, K. Y.; Nojiri, H.; Nakamoto, A.; Kojima, N.; Cimpoesu, F.; Fujimura, Y.; Takaishi, S.; Yamashita, M. *J. Am. Chem. Soc.* **2006**, *128*, 9008−9009. (e) Mori, F.; Nyui, T.; Ishida, T.; Nogami, T.; Choi, K.-Y.; Nojiri, H. *J. Am. Chem. Soc.* **2006**, *128*, 14408−14009. (f) Ishida, T.; Watanabe, R.; Fujiwara, K.; Okazawa, A.; Kojima, N.; Tanaka, G.; Yoshii, S.; Noriji, H. *Dalton Trans.* **2012**, *41*, 13609−13619. (g) Gao, Y.; Zhao, L.; Xu, X.; Xu, G.-F.; Guo, Y.-N.; Tang, J.; Liu, Z. *Inorg. Chem.* **2011**, *50*, 1304−1308. (h) Colacio, E.; Ruiz, J.; Mota, A. J.; Palacios, M. A.; Cremades, E.; Ruiz, E.; White, F. J.; Euan K. Brechin, E. K. *Inorg. Chem.* **2012**, *51*, 5857−5868. (i) Efthymiou, C. G.; Stamatatos, T. C.; Papatriantafyllopoulou, C.; Tasiopoulos, A. J.; Wernsdorfer, W.; Perlepes, S. P.; Christou, G. *Inorg. Chem.* **2010**, *49*, 9737−9739. (j) Burrow, C. E.; Burchell, T. J.; Lin, P.-H.; Habib, F.; Wernsdorfer, W.; Clérac, R.; Murugesu, M. *Inorg. Chem.* **2009**, *48*, 8051−8053. (k) Yamaguchi, T.; Sunatsuki, Y.; Ishida, H.; Kojima, M.; Akashi, H.; Re, N.; Matsumoto, N.; Pochaba, A.; Mrozinski, J. *Bull. Chem. Soc. Jpn.* **2008**, *81*, 598−605. (l) Hamamatsu, T.; Yabe, K.; Towatari, M.; Osa, S.; Matsumoto, N.; Re, N.; Pochaba, A.; Mrozinski, J.; Gallani, J. L.; Barla, A.; Imperia, P.; Paulsen, C.; Kappler, J. P. *Inorg. Chem.* **2007**, *46*, 4458−4468. (m) Sessoli, R.; Powell, A. K. *Coord. Chem. Rev.* **2009**, *253*, 2328−2341. (n) Costes, J. P.; Vendier, L.; Wernsdorfer, W. *Dalton Trans.* **2011**, *40*, 1700−1706. (o) Sakamoto, S.; Fujinami, T.; Nishi, K.; Matsumoto, N.; Mochida, N.; Ishida, T.; Sunatsuki, Y.; Re, N. *Inorg. Chem.* **2013**, *52*, 7218−7229.

(5) (a) Sorace, L.; Benelli, C.; Gatteschi, D. *Chem. Soc. Rev.* **2011**, *40*, 3092−3104. (b) Layfield, R. A.; McDouall, J. J. W.; Sulway, S. A.; Tuna, F.; Collison, D.; Winpenny, R. E. P. *Chem. Eur. J.* **2010**, *16*, 4442−4446. (c) Long, J.; Habib, F.; Lin, P.-H.; Korobkov, I.; Enright, G.; Ungur, L.; Wernsdorfer, W.; Chibotaru, L.; Murugesu, M. *J. Am. Chem. Soc.* **2011**, *133*, 5319−5328. (d) Guo, Y.-N.; Xu, G.-F.; Guo, Y.; Tang, J. *Dalton Trans.* **2011**, *40*, 9953−9963. (e) Hewitt, I. J.; Tang, J.; Madhu, N. T.; Anson, C. E.; Lan, Y.; Luzon, Y.; Etienne, M.; Sessoli, R.; Powell, A. K. *Angew. Chem., Int. Ed.* **2010**, *49*, 6352−6356. (f) Blagg, R. J.; Muryn, C. A.; McInnes, E. J. L.; Tuna, F.; Winpenny, R. E. P. *Angew. Chem., Int. Ed.* **2011**, *50*, 6530−6533. (g) Rhinehart, J. D.; Feng, M.; Evans, W. J.; Long, J. R. *J. Am. Chem. Soc.* **2011**, *133*, 14236−14239. (h) Zhang, P.; Guo, Y.-N.; Tang, J. *Coord. Chem. Rev.* **2013**, *257*, 1728−1763. (i) Luzon, J.; Sessoli, R. *Dalton Trans.* **2012**, *41*, 13556−13567. (j) Karbowiak, M.; Rudowicz, C.; Ishida, T. *Inorg. Chem.* **2013**, *52*, 13199−13206.

(6) (a) Lin, P.-H.; Burchell, T. J.; Clerac, R.; Murugesu, M. *Angew. Chem., Int. Ed.* **2008**, *47*, 8848−8851. (b) Hewitt, I. J.; Lan, Y.; Anson, C. E.; Luzon, J.; Sessoli, R.; Powell, A. K. *Chem. Commun.* **2009**, 6765−6767. (c) Guo, Y.-N.; Xu, G.-F.; Wernsdorfer, W.; Ungur, L.; Guo, Y.; Tang, J.; Zhang, H.-J.; Chibotaru, L. F.; Powell, A. K. *J. Am. Chem. Soc.* **2011**, *133*, 11948−11951. (d) Zhang, P.; Zhang, L.; Lin, S.-Y.; Tang, J. *Inorg. Chem.* **2013**, *52*, 6595−6602.

(7) (a) Petoud, S.; Muller, G.; Moore, E. G.; Xu, J.; Sokolnicki, J.; Riehl, J. P.; Le, U. N.; Cohen, S. M.; Raymond, K. N. *J. Am. Chem. Soc.*

2007, *129*, 77−83. (b) Pasatoiu, T. D.; Tiseanu, C.; Maladan, A. M.; Jurca, B.; Duhayon, C.; Sutter, J. P.; Andruh, M. *Inorg. Chem.* **2011**, *50*, 5879−5889. (c) Titos-Padilla, S.; Ruiz, J.; Herrera, J. M.; Brechin, E. K.; Wersndorfer, W.; Lloret, F.; Colacio, E. *Inorg. Chem.* **2013**, *52*, 9620−9626. (d) Wang, Y.-L.; Ma, Y.; Yang, X.; Tang, J.; Cheng, P.; Wang, Q.-L.; Li, L.-C.; Liao, D.-Z. *Inorg. Chem.* **2013**, *52*, 7380−7386. (e) Biju, S.; Gopakumar, N.; Bünzli, J.-C. G.; Scopelliti, R.; Kim, H. K.; Reddy, M. L. P. *Inorg. Chem.* **2013**, *52*, 8750−8756. (f) Li, Q.-W.; Liu, J.-L.; Ja, J.-H.; Leng, J.-D.; Lin, W.-Q.; Chen, Y.-C.; Tong, M.-L. *Dalton Trans.* **2013**, *42*, 11262−11270.

(8) (a) Cucinotta, G.; Perfetti, M.; Luzon, J.; Etienne, M.; Car, P.-E.; Caneschi, A.; Calvez, G.; Bernot, K.; Sessoli, R. *Angew. Chem., Int. Ed.* **2012**, *51*, 1606−1610. (b) Long, J.; Rémi, V.; Ferreira, R. A. S.; Carlos, L. D.; Paz, F. A. A.; Guari, Y.; Larionova, J. *Chem. Commun.* **2012**, *48*, 9974−9976.

(9) (a) Yamauchi, S.; Hashibe, T.; Murase, M.; Hagiwara, H.; Matsumoto, N.; Tsuchimoto, M. *Polyhedron* **2013**, *49*, 105−112. (b) Yamauchi, S.; Fujinami, T.; Matsumoto, N.; Mochida, N.; Ishida, T.; Sunatsuki, Y.; Watanabe, M.; Tsuchimoto, M.; Coletti, C.; Re, N. *Inorg. Chem.* **2014**, *53*, 5961−5971.

(10) (a) Katsuki, I.; Motoda, Y.; Sunatsuki, Y.; Matsumoto, N.; Nakashima, T.; Kojima, M. *J. Am. Chem. Soc.* **2002**, *124*, 629−640. (b) Katsuki, I.; Matsumoto, N.; Kojima, M. *Inorg. Chem.* **2000**, *39*, 3350−3354. (c) Ikuta, Y.; Ooidemizu, M.; Yamahata, Y.; Yamada, M.; Osa, S.; Matsumoto, N.; Iijima, S.; Sunatsuki, Y.; Kojima, M.; Dahan, F.; Tuchagues, J. P. *Inorg. Chem.* **2003**, *42*, 7001−7012. (d) Yamada, M.; Hagiwara, H.; Torigoe, H.; Matsumoto, N.; Kojima, M.; F. Dahan, F.; Tuchagues, J. P.; Re, N.; Iijima, S. *Chem. Eur. J.* **2006**, *12*, 4536−4549. (e) Brewer, C.; Brewer, G.; Luckett, C.; Marbury, G. S.; Viragh, C.; Beatty, A. M.; Scheidt, W. R. *Inorg. Chem.* **2004**, *43*, 2402−2415. (f) Brewer, C.; Brewer, G.; Butcher, R. J.; Carpenter, E. E.; Cuenca, L.; Noll, B. C.; Scheidt, W. R.; Viragh, C.; Zavalij, P. Y.; Zielaski, D. *Dalton Trans.* **2006**, 1009−1019.

(11) (a) Nakamura, H.; Fujii, M.; Sunatsuki, Y.; Kojima, M.; Matsumoto, N. *Eur. J. Inorg. Chem.* **2008**, 1258−1267. (b) Sunatsuki, Y.; Ohta, H.; Kojima, M.; Ikuta, Y.; Goto, Y.; Matsumoto, N.; Iijima, S.; Akashi, H.; Kaizaki, S.; Dahan, F.; Tuchagues, J.-P. *Inorg. Chem.* **2004**, *43*, 4154−4171. (c) Yamada, M.; Ooidemizu, M.; Ikuta, Y.; Osa, S.; Matsumoto, N.; Iijima, S.; Kojima, M.; Dahan, F.; Tuchagues, J.-P. *Inorg. Chem.* **2003**, *42*, 8406−8416. (d) Sunatsuki, Y.; Ikuta, Y.; Matsumoto, N.; Ohta, H.; Kojima, M.; Iijima, S.; Hayami, S.; Maeda, Y.; Kaizaki, S.; Dahan, F.; Tuchagues, J.-P. *Angew. Chem., Int. Ed.* **2003**, *42*, 1614−1618. (e) Nagasato, S.; Sunatsuki, Y.; Ohsato, S.; Kido, T.; Matsumoto, N.; Kojima, M. *Chem. Commun.* **2002**, 14−15.

(12) Murase, M.; Yamauchi, S.; Sakamoto, S.; Takahashi, S.; Matsumoto, N.; Tsuchimoto, M. *Polyhedron* **2013**, *59*, 76−84.

(13) (a) Takahashi, S.; Hashimoto, S.; Shimogori, S.; Matsumoto, N.; Nakashima, T.; Tsuchimoto, M. *Polyhedron* **2011**, *30*, 2026−2031. (b) Takahashi, S.; Murase, M.; Hagiwara, H.; Matsumoto, N.; Tsuchimoto, M. *Bull. Chem. Soc. Jpn.* **2011**, *84*, 1082−1089.

(14) Kahn, O. *Molecular Magnetism*; VCH: Weinheim, Germany, 1993; Chapter 1, Table I.1.

(15) (a) SIR92: Altomare, A.; Cascarano, G.; Giacovazzo, C.; Guagliardi, A.; Burla, M.; Polidori, G.; Camalli, M. *J. Appl. Crystallogr.* **1994**, *27*, 435. (b) DIRDIF-99: , Beurskens, P. T.; Admiraal, G.; Beurskens, G.; Bosman, W. P.; de Gelder, R.; Israel, R.; Smits, J. M. M. *The DIRDIF-99 program system,* , Technical Report of the Crystallography Laboratory; University of Nijmegen, Nijmegen, The Netherlands, 1999.

(16) *CrystalStructure 4.0: Crystal Structure Analysis Package*, Rigaku Corporation, Tokyo, Japan, 2000−2010.

(17) *Jaguar, version 7.9,*; Schrödinger, LLC, New York, NY, 2011.

(18) Grimme, S.; Antony, J.; Ehrlich, S.; Krieg, H. *J. Chem. Phys.* **2010**, *132*, 1541041-1−154104-19.

(19) Cundari, T. R.; Stevens, W. J. *J. Chem. Phys.* **1993**, *98*, 5555−5565.

(20) Llunell, M.; Casanova, D.; Cirera, J.; Alemany, P.; Alvarez, S. *SHAPE, v2.1*; University of Barcelona and The Hebrew University of Jerusalem, Barcelona and Jerusalem, 2013.

(21) Drew, M. G. B. *Coord. Chem. Rev.* **1977**, *24*, 179−275.

(22) Abragam, A.; Bleaney, B. *Electron Paramagnetic Resonance*; Clarendon Press: Oxford, U.K., 1970.

(23) Stevens, K. W. H. *Proc. Phys. Soc.* **1952**, *A65* (3), 209−215.

(24) (a) AlDamen, M. A.; Cardona-Serra, S.; Clemente-Juan, J. M.; Coronado, E.; Gaita-Ariño, A.; Martì-Gastaldo, C.; Luis, F.; Montero, O. *Inorg. Chem.* **2009**, *48*, 3467−3479. (b) Chandrasekhar, V.; Bag, P.; Speldrich, M.; van Leusen, J.; Kögerler, P. *Inorg. Chem.* **2013**, *52*, 5035−5044. (c) Yamaguchi, T.; Sunatsuki, Y.; Ishida, H.; Kojima, M.; Akashi, H.; Re, N.; Matsumoto, N.; Pochaba, A.; Mrozinski, J. *Inorg. Chem.* **2008**, *47*, 5736−5745. (d) Kajiwara, T.; Nakano, M.; Takaishi, S.; Yamashita, M. *Inorg. Chem.* **2008**, *47*, 8604−8606. (e) Kajiwara, T.; Takahashi, K.; Hiraizumi, T.; Takaishi, S.; Yamashita, M. *Cryst. Eng. Commun.* **2009**, *11*, 2110−2116. (f) Kajiwara, T.; Nakano, M.; Takahashi, K.; Takaishi, S.; Yamashita, M. *Chem. Eur. J.* **2011**, *17*, 196−205. (g) Ehama, K.; Ohmichi, Y.; Sakamoto, S.; Fujinami, T.; Matsumoto, N.; Mochida, N.; Ishida, T.; Sunatsuki, Y.; Tsuchimoto, M.; Re, N. *Inorg. Chem.* **2013**, *52*, 12828−12841. (h) Yamashita, K.; Miyazaki, R.; Kataoka, Y.; Nakanishi, T.; Hasegawa, Y.; Nakano, M.; Yamamura, T.; Kajiwara, T. *Dalton Trans.* **2013**, *42*, 1987−1990. (i) Przychodzeń, P.; Pełka, R.; Leviński, K.; Supel, J.; Rams, M.; Tomala, K.; Sieklucka, B. *Inorg. Chem.* **2007**, *46*, 8924−8938.

(25) Bartolomé, J.; Filoti, G.; Kuncser, V.; Schinteie, G.; Mereacre, V.; Anson, C. E.; Powell, A. K.; Prodius, D.; Turta, C. *Phys. Rev. B* **2009**, *80*, 014430 (16 pages).

(26) (a) Sievers, J. *Z. Phys. B: Condens. Matter Quanta* **1982**, *45*, 2689−296. (b) Schmitt, D. *J. Phys. (Paris)* **1986**, *47*, 677−681. (c) Rinehart, J. D.; Long, J. R. *Chem. Sci.* **2011**, *2*, 2078−2085. (d) Aravena, D.; Ruiz, E. *Inorg. Chem.* **2013**, *52*, 13770−13778. (e) Chilton, N. F.; Collison, D.; McInnes, E. J. L.; Winpenny, R. E. P.; Soncini, A. *Nat. Commun.* **2013**, *4*, 2551 (7 pages).

■ NOTE ADDED AFTER ASAP PUBLICATION

This paper was published on the Web on September 9, 2014. References 12b and 12c were deleted, and the corrected version was reposted on September 15, 2014.